

Coefficient Shape Transfer Learning for Functional Linear Regression

Shuhao Jiao^{*1}, Ian W. McKeague², and Ngai Hang Chan¹

¹*Department of Biostatistics, City University of Hong Kong*

²*Department of Biostatistics, Columbia University*

Abstract

The shapes of functions provide highly interpretable summaries of their trajectories. This article develops a novel transfer learning framework for functional linear regression that leverages coefficient shape information to overcome data scarcity. The proposed methodology integrates samples from the target model (target domain) with those from auxiliary models (source domains), enabling effective knowledge transfer across heterogeneous data sources. This shape-based transfer learning framework enhances robustness and generalizability: by being invariant to covariate scaling and signal strength, it ensures reliable knowledge transfer even when data from different sources differ in magnitude, and by formalizing the notion of coefficient shape homogeneity, it extends beyond traditional coefficient-equality assumptions to incorporate information from a broader range of source domains. We establish non-asymptotic convergence rates and minimax optimality of the estimator, showing that improvement depends on shape similarity, coefficient magnitude, and spectral decay rates of the covariance operators of covariates across different domains. A data-driven source domain selection procedure is developed to identify informative auxiliary domains. Simulations and a real data application to physical activity data from the U.S. National Health and Nutrition Examination Survey demonstrate the framework's accuracy, robustness, and interpretability.

Keywords: Coefficient shape, Functional linear regression, Minimax optimality, Non-asymptotic convergence, Transfer learning.

*Corresponding Author: shuhao.jiao@cityu.edu.hk

1 Introduction

1.1 Background

Machine learning techniques have achieved significant success in many practical problems. However, a common assumption in machine learning is that both training and test data come from the same distribution. Consequently, when new data from a different distribution is encountered, statistical models often need to be redeveloped from scratch. In many scenarios, re-collecting training data and rebuilding models is costly or impractical. Therefore, there is a growing demand to utilize existing datasets to aid in the development of new models, leading to the emergence of transfer learning. Transfer learning leverages knowledge gained from solving auxiliary problems and applies it to a new one. This technique draws inspiration from the human ability to apply previously acquired knowledge to improve performance on new tasks. Transfer learning has been applied in many fields, such as neuroimaging analysis (see e.g., [1]), image classification (see e.g., [12, 22]), natural language processing (see e.g., [9]), protein function prediction (see e.g., [15]), functional data analysis (see e.g., [5], [20], [16], [21]), and high-dimensional regression (see e.g., [3], [19] and [29])

Functional data analysis (FDA) encompasses a variety of statistical methods used to analyze data represented as functions, images, shapes, or more general objects (see e.g., [31]). Coefficient homogeneity has been employed to build parsimonious models (see, e.g., [28], [23], and [27]), and can be readily adopted in transfer learning by assuming that models across different domains share similar coefficients. Two pioneering papers, [20] and [16], have made important contributions along this line of research. *A major and critical drawback* of the coefficient homogeneity assumption is its lack of robustness to data scaling: scaling can dramatically distort the differences between associated coefficients, leading to inconsistent and unreliable transfer of knowledge on coefficient amplitude across domains. This issue is particularly pronounced in transfer learning because source domains with high data variability can easily dominate those with lower variability, making data scaling unavoidable in many practical applications. Moreover, it reduces generalization and interpretability, as the equality constraint suppresses structural variations across domains—treating all coefficients as identical prevents the model from capturing shared but non-identical association patterns. In contrast, this paper develops a new transfer learning methodology based on *coefficient shape similarity*, which effectively overcomes the inherent weaknesses of the coefficient homogeneity assumption. It is worth noting that, while both [20] and our work study the impact of signal strength on transfer learning, their work builds on coefficient homogeneity whereas ours emphasizes coefficient shape similarity, and the two works offer complementary insights on the transferred knowledge in the setting of functional linear model.

1.2 Problem of Interest

We now present the problem setup. Since the intercept does not affect the convergence rate of the coefficient functions (see e.g., [10]), for simplicity we assume that the mean of response and functional covariate variables are both zero, and the target model of interest is given by

$$y_n^{(0)} = \langle X_n^{(0)}, \beta^{(0)} \rangle + \epsilon_n^{(0)}, \quad n = 1, \dots, N_0, \quad \epsilon_n^{(0)} \stackrel{i.i.d.}{\sim} \text{subG}(\sigma^2), \quad (1-1)$$

in which $\epsilon_n^{(0)} \sim \text{subG}(\sigma^2)$ indicates that $\epsilon_n^{(0)}$ follows a sub-Gaussian distribution with variance proxy σ^2 , and are independent across n . Here $\langle \cdot, \cdot \rangle$ denotes the inner product in $L^2[0, 1]$, $X_n^{(0)}(t)$ denotes the square-integrable functional covariate of the target model, and $\beta^{(0)}(t)$ denotes the associated unknown coefficient function. In addition, assume that we have data generated from p auxiliary models as follows,

$$y_n^{(j)} = \langle X_n^{(j)}, \beta^{(j)} \rangle + \epsilon_n^{(j)}, \quad n = 1, \dots, N_j, \quad \epsilon_n^{(j)} \stackrel{i.i.d.}{\sim} \text{subG}(\sigma^2), \quad j = 1, \dots, p, \quad (1-2)$$

where $\beta^{(j)}(t)$ is the unknown coefficient functions of the j 's auxiliary model. It is assumed that for some j 's, the function $\beta^{(j)}(t)$ shares a similar coefficient shape with $\beta^{(0)}(t)$, and the set of these domains, denoted by \mathcal{A} , is termed the *informative set*.

A transfer learning procedure is composed of two steps: pre-training and fine-tuning. Generally, for some known functional $f(\cdot)$, let $\beta^{(0)}(t) = f(\beta^c, a_0)(t)$, where $\beta^c(t)$ represents the transferred knowledge that is to be estimated from the data in \mathcal{A} and the target domain in the pre-training step, and a_0 accounts for the divergence between $\beta^{(0)}(t)$ and $\beta^c(t)$, being estimated in the fine-tuning step. After obtaining $\hat{\beta}^c(t)$ and \hat{a}_0 in the two aforementioned steps, the final estimator of $\beta^{(0)}(t)$ is given by $\hat{\beta}^{(0)}(t) = f(\hat{\beta}^c, \hat{a}_0)(t)$.

1.3 Our Contributions

The fundamental contribution of this paper is the development of a novel transfer learning methodology that leverages coefficient shape to enhance the estimation of the target functional linear regression model. Coefficient shape learning targets the geometry of functional effect patterns—peaks, supports, and trends of coefficient functions—rather than only their pointwise magnitudes. In functional linear models, the shapes are highly interpretable summaries of how an entire covariate trajectory drives an outcome. In real-world settings—such as neuroimaging, motion monitoring, or wearable-sensor systems—individuals often exhibit common activity patterns. What distinguishes them is the shape of their trajectories—when peaks occur, how sharply they rise or fall, and how long plateaus persist. A shape-based modeling approach captures precisely these structural characteristics. By focusing on geometry rather than magnitude, it adapts naturally to differences in signal strength. Consequently, this approach not only enhances the performance of the target model but also ensures that the underlying association patterns remain comparable and interpretable across domains. In summary, by modeling, aligning, and transferring function shapes, we gain three major pay-offs: (i) stability—shape information is more robust to data scaling and magnitude variation;

(ii) interpretability—localized peaks and sustained plateaus translate into clear mechanistic claims; and (iii) generalization—in contrast to coefficient-equality-based methods, our shape-based transfer learning framework flexibly incorporates information from more source domains, enhancing adaptability and predictive accuracy.

The principle is that, if the j -th auxiliary model is close to the target model, the coefficient shape of the two models should be similar, in the sense that $\beta^{(j)}(t) \approx \text{const.} \beta^{(0)}(t)$. Clearly, while two functions are of the same shape if they are equal, two functions of the same shape are not necessarily identical. Therefore, this new principle enables the incorporation of information from a broader range of source domains, thereby enhancing model estimation. More importantly, coefficient shape homogeneity is *invariant* to covariate scaling, addressing the crucial limitations of coefficient homogeneity principle discussed in Section ???. The developed transfer learning procedure is able to yield significantly greater improvements than merely increasing the target domain’s sample size. Due to the infinite-dimensional nature of functional data, the prediction mean squared error of the ordinary least squares estimator decays at a rate slower than $O(N_0^{-1})$. Under suitable conditions on the source domains, this rate can be improved to $O((N_{\mathcal{A}} + N_0)^{-1})$ or faster, where $N_{\mathcal{A}} = \sum_{j \in \mathcal{A}} N_j$. In principle, when the source domains exhibit similar coefficient shapes, slow spectral decay, and large coefficient magnitudes, the proposed transfer learning method yields greater improvements than simply increasing the sample size in the target domain. For the case where \mathcal{A} is unknown, a data-driven approach is developed to identify it. To this end, we introduce a novel shape misalignment measure, which quantifies the discrepancy in coefficient shapes between the source domains and the target domain. Based on this measure, we define the informative set as the collection of source domains exhibiting sufficiently small shape misalignment. The identification is formulated as a regularized optimization problem with a concave penalty, and we show that this approach yields consistent identification of the true informative set under some regularity conditions.

The rest of the paper is organized as follows. In Section 2, we develop the new transfer learning methodology based on coefficient shape homogeneity, and we also establish the convergence rates of the final estimator and study the minimax optimality. In Section 3, we develop an identification method for the unknown informative set, and investigate the consistency property of the identification result. Finite-sample properties of the proposed methods are investigated through simulation studies in Section 4. A case study of the association between age and physical activity levels using occupation time curves as covariates is provided in Section 5. Section 6 concludes the paper. Technical proofs and algorithms are given in the appendix.

2 Coefficient Shape Transfer Learning

2.1 Preliminaries

The coefficient and covariate functions are assumed to belong to $L^2[0, 1]$, in which the inner product is defined as $\langle x, y \rangle = \int_0^1 x(t)y(t) dt$, and the L^2 -norm is defined by $\|x\|^2 = \int_0^1 x^2(t) dt < \infty$. Suppose that there is a target data source including N_0 observations $\{(X_n^{(0)}(t), y_n^{(0)}) : n = 1, \dots, N_0\}$ following the model (1-1), and, in addition, there are p auxiliary data sources, where in the j -th source the N_j observations $\{(X_n^{(j)}(t), y_n^{(j)}) : n = 1, \dots, N_j\}$ follow model (1-2). The (empirical) covariance operator of the design covariates $\{X_n^{(j)}(t) : n = 1, \dots, N_j\}$ is defined as $\mathcal{C}_j(x)(t) = \int C_j(t, s)x(s)ds$, where $C_j(t, s) = N_j^{-1} \sum_{n=1}^{N_j} \{X_n^{(j)} - \bar{X}^{(j)}\}(t)\{X_n^{(j)} - \bar{X}^{(j)}\}(s)$, and $\bar{X}^{(j)}(t) = N_j^{-1} \sum_{n=1}^{N_j} X_n^{(j)}(t)$, for $j = 0, \dots, p$. For simplicity, we assume that $\bar{X}^{(j)}(t) = 0$ for all j 's. It is readily checked that each $\mathcal{C}_j(\cdot)$ is a compact operator on $L^2[0, 1]$.

Our objective is to fit the target model $y_n^{(0)} = \langle X_n^{(0)}, \beta^{(0)} \rangle + \epsilon_n^{(0)}$, where $\beta^{(0)}(t) \in L^2[0, 1]$. By an extension of Mercer's theorem to compact covariance operators due to Baker and McKeague [2], and the corresponding Karhunen–Loève representation theorem, we have the following functional principal component decompositions

$$\mathcal{C}_0(\cdot) = \sum_{d \geq 1} \theta_{0d} \langle \nu_d, \cdot \rangle \nu_d(t), \quad X_n^{(0)}(t) = \sum_{d \geq 1} \xi_{nd}^{(0)} \nu_d(t) = \sum_{d \geq 1} \langle X_n^{(0)}, \nu_d \rangle \nu_d(t),$$

where $\{(\theta_{0d}, \nu_d(t)) : d \geq 1\}$ are the eigenpairs of $\mathcal{C}_0(\cdot)$. Although technically $\mathcal{C}_0(\cdot)$ depends on the sample size N_0 , as we argue in Remark 3 below it is reasonable to assume that the target coefficient function belongs to an “enhanced” parameter space (see also e.g., Cai and Hall [4], Hall and Horowitz [14] and Jiao et al. [17]):

$$\Theta_\beta = \left\{ \beta(t) \in L^2[0, 1] : \beta(t) = \sum_{d \geq 1} b_{0d} \nu_d(t), \sum_{d \geq 1} b_{0d}^2 < \infty \right\}.$$

More generally, Yuan and Cai [33] and Cai and Yuan [6] examined the scenario in which the reproducing kernel associated with the coefficient function is not necessarily well aligned with the covariance kernel of the functional covariate, but we do not pursue that direction here.

Remark 1. It is assumed that the variance of $\epsilon_n^{(j)}$ is the same for all $j = 0, 1, \dots, p$. This assumption is reasonable in the context of the article for two reasons: 1) the error variance of different sources can always be scaled to a common level, and 2) the coefficient shape is invariant to data scaling.

In the sequel, we use “ c ” to denote generic positive constants. Let $a_n \asymp b_n$ denote $c^{-1}b_n < a_n \leq cb_n$ for some $c > 1$, $a_n \lesssim b_n$ denote $a_n \leq cb_n$ for some $c > 0$, and $a_n \gtrsim b_n$ denote $a_n \geq cb_n$ for some $c > 0$.

2.2 Coefficient Shape Misalignment and Informative Set

For the auxiliary models, assume that the coefficients and covariates admit the following basis representations $\beta^{(j)}(t) = \sum_{d \geq 1} b_{jd} \nu_d(t)$, $X_n^{(j)}(t) = \sum_{d \geq 1} \xi_{nd}^{(j)} \nu_d(t)$. To evaluate coefficient shape discrepancy, we define the *coefficient shape misalignment* between $\beta^{(j)}(t)$ and $\beta^{(0)}(t)$ as $\mathcal{M}_j = \{M_{dd'}^{(j)}, 1 \leq d < d'\}$, where $M_{dd'}^{(j)} = b_{jd} b_{0d'} - b_{jd'} b_{0d}$. Notably, when $\|\mathcal{M}_j\|^2 = \sum_{d < d'} \{M_{dd'}^{(j)}\}^2 = 0$, $\beta^{(j)}(t) = c\beta^{(0)}(t)$. It is important to recognize that $\|\mathcal{M}_j\|$ can be small simply due to $\|\beta^{(j)}\|$ being small. To eliminate the influence of coefficient magnitude and ensure robust identification of the informative set, we define \mathcal{A} with a threshold $\tilde{\lambda} \geq 0$ as

$$\mathcal{A} = \{j: \|\mathcal{M}_j\| \leq \tilde{\lambda} \|\beta^{(j)}\| \|\beta^{(0)}\|\}.$$

The informative set is *robust* to covariate scaling because $\|\mathcal{M}_j\|/(\|\beta^{(j)}\| \|\beta^{(0)}\|)$ remains unchanged if the covariate functions are scaled to $c_0 X_n^{(j)}(t)$ and $c'_0 X_n^{(0)}(t)$, while accordingly the associated coefficient functions are scaled to $c_0^{-1} \beta^{(j)}(t)$ and $c'^{-1}_0 \beta^{(0)}(t)$ with arbitrary constants $c_0, c'_0 \in \mathbb{R} \setminus \{0\}$. The tuning parameter $\tilde{\lambda}$ controls the coefficient shape similarity between the target model and the auxiliary models, with a larger $\tilde{\lambda}$ leading to a more extensive informative set. It will be seen later that when $\tilde{\lambda}$ is sufficiently small, the information in \mathcal{A} contributes to improving the estimation of $\beta^{(0)}(t)$. This parameter will be selected using a cross-validation method, as discussed in Section 3.

Remark 2. Generally, the covariates and coefficients in the auxiliary models admit the orthogonal decompositions $\beta^{(j)}(t) = \sum_{d \geq 1} b_{jd} \nu_d(t) + \eta_j(t)$, $X_n^{(j)}(t) = \sum_{d \geq 1} \xi_{nd}^{(j)} \nu_d(t) + Z_n^{(j)}(t)$, where $\eta_j(t), Z_n^{(j)}(t) \in \Theta_\beta^\perp \subset L^2[0, 1]$, and Θ_β^\perp is the orthogonal component of Θ_β . The components $Z_n^{(j)}, \eta_j$, assumed to be irrelevant to the target model, and are not incorporated in knowledge transfer. Thus, in practice, we use $\{\nu_d(t): d \geq 1\}$ as basis functions to construct approximations for $\beta^{(j)}(t)$ and $X_n^{(j)}(t)$, making the assumptions $\beta^{(j)}(t) = \sum_{d \geq 1} b_{jd} \nu_d(t)$, $X_n^{(j)}(t) = \sum_{d \geq 1} \xi_{nd}^{(j)} \nu_d(t)$ reasonable.

2.3 Estimation with Transferred Coefficient Shape

In this section, we develop the estimation procedure. We assume that the coefficient function of the target model admits the decomposition $\beta^{(0)}(t) = a_0 \beta^c(t)$. Here $\beta^c(t)$ is termed the coefficient shape component, and a_0 is termed the coefficient amplitude component. In addition, each coefficient function of the auxiliary models admits the decomposition

$$\beta^{(j)}(t) = a_j \{\beta^c(t) + h_j(t)\}, \text{ where } \langle \beta^c, h_j \rangle = 0, h_j(t) \in \Theta_\beta.$$

This decomposition is not identifiable, because $\beta^{(j)}(t) = (ra_j)[r^{-1}\{\beta^c(t) + h_j(t)\}]$ for arbitrary $r \neq 0$. For identifiability and consistency, it is required that $\beta^c(t) = \sum_{j \in \mathcal{A} \cup \{0\}} \omega_j \beta^{(j)}(t)$ if $h_j(t) = 0$ for $j \in \mathcal{A}$ (note that this does *not* mean we assume $h_j(t) = 0$ for $j \in \mathcal{A}$), and

impose the restriction $\sum_{j \in \mathcal{A} \cup \{0\}} \omega_j a_j = 1$. Under this restriction, we equivalently have that, if $h_j(t) = 0$ for $j \in \mathcal{A}$,

$$\beta^c(t) = \sum_{j \in \mathcal{A} \cup \{0\}} \omega_j \sum_{d \geq 1} b_{jd} \nu_d(t) \triangleq \sum_{d \geq 1} b_d^c \nu_d(t),$$

where $b_d^c = \sum_{j \in \mathcal{A} \cup \{0\}} \omega_j b_{jd}$. Note that the coefficient shape component $\beta^c(t)$ is shared by the target model and the auxiliary models, making it possible to use the samples in the source domains to improve the estimation of $\beta^c(t)$, provided that $\|a_j h_j\|$ are sufficiently small for $j \in \mathcal{A}$. Then we adjust the amplitude of the target coefficient to get the final estimator of $\beta^{(0)}(t)$. Now we present the transfer learning procedure:

Pre-training step. We estimate the coefficient functions of the target and related auxiliary models

$$\check{\beta}^{(j)}(t) = \arg \min_{\beta(t) \in \Theta_\beta} \sum_{n=1}^{N_j} \{y_n^{(j)} - \langle X_n^{(j)}, \beta \rangle\}^2, \quad j \in \mathcal{A} \cup \{0\}.$$

The least squares estimation is performed after projection onto the basis $\{\nu_d(t) : d \geq 1\}$ (see e.g., Cai and Hall [4] and Hall and Horowitz [14]). Using the basis representation, we derive the multivariate regression form of the functional model $y_n^{(j)} = \sum_{d \geq 1} \xi_{nd}^{(j)} b_{jd} + \epsilon_n^{(j)} = \sum_{d=1}^D \xi_{nd}^{(j)} b_{jd} + \tilde{\epsilon}_n^{(j)}$, where $\tilde{\epsilon}_n^{(j)} = \epsilon_n^{(j)} + \sum_{d \geq D+1} \xi_{nd}^{(j)} b_{jd}$ for some sufficiently large $D \geq 1$. Then we use the least squares method to obtain the pre-estimate $\check{\mathbf{b}}_j = (\check{b}_{j1}, \dots, \check{b}_{jD})$, and the resulting estimate of $\beta^{(j)}(t)$ is given by $\check{\beta}^{(j)}(t) = \sum_{d=1}^D \check{b}_{jd} \nu_d(t)$. Then we estimate the coefficient shape component as follows

$$\hat{\beta}^c(t) = \sum_{j \in \mathcal{A} \cup \{0\}} \omega_j \check{\beta}^{(j)}(t), \quad \omega_j = \text{sign}(\langle \check{\beta}^{(j)}, \check{\beta}^{(0)} \rangle) \times \frac{N_j}{N_{\mathcal{A}} + N_0},$$

where $N_{\mathcal{A}} = \sum_{j \in \mathcal{A}} N_j$. We estimate the coefficient function separately in each domain, eliminating the need to re-estimate $\beta^c(t)$ from scratch when incorporating a new source domain, thereby significantly reducing the computational burden.

Fine-tuning step. We estimate the coefficient amplitude based on $\hat{\beta}^c(t)$ as follows

$$\hat{a}_0 = \arg \min_{a_0 \in \mathbb{R}} \sum_{n=1}^{N_0} \left\{ y_n^{(0)} - a_0 \langle X_n^{(0)}, \hat{\beta}^c \rangle \right\}^2.$$

Then the final estimator of the target coefficient function is $\hat{\beta}^{(0)}(t) = \hat{a}_0 \hat{\beta}^c(t)$.

In the pre-training step, we estimate the coefficient shape component using all samples from the source domains within the informative set, and $\hat{\beta}^c(t)$ serves as a reliable estimator of $\beta^c(t)$ when $\tilde{\lambda}$ is small. The probability limit of $\hat{\beta}^c(t)$ is $\sum_{j \in \mathcal{A} \cup \{0\}} \omega_j \beta^{(j)}(t) = \beta^c(t) + \sum_{j \in \mathcal{A} \cup \{0\}} \omega_j a_j h_j(t)$. As a special case, when $\tilde{\lambda} = 0$, the estimator $\hat{\beta}^c(t)$ is consistent for $\beta^c(t)$ as $N, D \rightarrow \infty$. Notably, when the source domains are sufficiently informative and $N_{\mathcal{A}} \gg N_0$, the convergence rate of $\hat{\beta}^c(t)$ is expected to be substantially faster than that of

the ordinary least squares estimator using only target domain samples. In the fine-tuning step, we further estimate the coefficient amplitude. The estimator \hat{a}_0 achieves a convergence rate of $O_p(N_0^{-1/2})$, which again surpasses that of the ordinary least squares estimator on the target domain alone, owing to the fact that a_0 is a scalar. Therefore, with a properly chosen $\tilde{\lambda}$, the convergence rate $\hat{\beta}^{(0)}(t)$ is expected to be significantly faster the estimators based solely on the target domain. A detailed discussion is provided below.

2.4 Theoretical Properties of the Final Estimator

2.4.1 Homogeneous Design

For simplicity in deriving the convergence rate of the transfer learning estimator, in this section we assume that there is only one source domain in \mathcal{A} (say, $\mathcal{A} = \{1\}$), and $\mathcal{C}_1(\cdot)$ and $\mathcal{C}_0(\cdot)$ are perfectly aligned, that is, $\mathcal{C}_1(\cdot) = \sum_{d \geq 1} \theta_{1d} \langle \nu_d, \cdot \rangle \nu_d(t)$ with $\theta_{11} \geq \theta_{12} \geq \dots$ being the eigenvalues of $\mathcal{C}_1(\cdot)$. Notationally, let $\|\hat{\beta}^{(0)} - \beta^{(0)}\|_{\mathcal{C}_0}^2 = \langle \hat{\beta}^{(0)} - \beta^{(0)}, \mathcal{C}_0(\hat{\beta}^{(0)} - \beta^{(0)}) \rangle$ to evaluate the prediction error. Here, $\|\beta^{(0)}\|$ is treated as fixed, whereas the magnitude of the source domain coefficient $\|\beta^{(1)}\|$ is allowed to vary.

To better understand the influence of source domain on the overall convergence rate, we consider the regime in which the source domain plays a dominant role in determining the convergence rate. To streamline the discussion, we assume that the design functions $\{X_n^{(j)}(t): j \in \mathcal{A} \cup \{0\}\}$ are non-random to underscore the core factors governing convergence behavior. The extension to the random design setting is presented in the supplementary material.

We first make the following assumptions.

- (A1) For $j = 0, 1$, $\{\epsilon_n^{(j)}: n = 1, \dots, N_j\}$ are independent zero-mean and sub-Gaussian with variance proxy σ^2 , meaning that $P\{|\sum_{n=1}^{N_j} s_n \epsilon_n^{(j)}| > t\} \leq 2 \exp(-t^2/2\sigma^2\|\mathbf{s}\|^2)$ for any $\mathbf{s} = (s_1, \dots, s_{N_j})$.
- (A2) For $n \geq 1$, $j = 0, 1$, $\xi_{nd}^{(j)} \lesssim d^{-\alpha_j/2}$ and $\theta_{jd} \asymp d^{-\alpha_j}$ with $\alpha_j > 1$, and $b_{0d} \lesssim d^{-\tilde{\alpha}_0}$ with $\tilde{\alpha}_0 > 1/2$.

Assumption (A1) posits sub-Gaussian random noise in both the primary and informative auxiliary samples, along with a finite second moment for the response vector. Assumption (A2) specifies the decaying rate of the covariate scores and the coefficient template scores. The assumption that $\alpha_j > 1$ and $\tilde{\alpha}_j > 1/2$ arises from the requirement that all functional elements are square-integrable.

Remark 3. As mentioned in the preliminary, it is reasonable to assume $\beta^{(0)}(t) \in \Theta_\beta$. It is mainly because the eigenfunctions $\{\nu_d(t): d \geq 1\}$ leads to stable scores as sample sizes diverge. Under a random design and some mild conditions on α_j , $\tilde{\alpha}_j$, it can be shown

that $|\theta_{jd} - \tilde{\theta}_{jd}| \leq \frac{1}{2}\tilde{\theta}_{jd}$ (this property is often used in existing literature, see e.g., Cai and Hall [4] and Hall and Horowitz [14]) and $|b_{jd} - \tilde{b}_{jd}| \leq \frac{1}{2}\tilde{b}_{jd}$ asymptotically almost surely for $j = 1, \dots, D$, where $\tilde{\theta}_{jd}$ and \tilde{b}_{jd} denote the counterparts of θ_{jd} and b_{jd} constructed using the eigenfunctions of $E\{\mathcal{C}_0(\cdot)\}$. This implies that, as the sample size grows, the decay rates of these scores remain stable. In this section, we focus on the scenario where this stability holds, in order to highlight the primary factors influencing the convergence rate. It is found that, under some regularity conditions (e.g., when the coefficient functions are sufficiently smooth), the convergence rate obtained under the random design setting coincides with that under the fixed design. More details are provided in the supplementary material.

We find that the transfer learning performance is affected by five factors: 1) the spectral decay rates of $\mathcal{C}_0(\cdot)$ and $\mathcal{C}_1(\cdot)$; 2) the coefficient magnitude in both target and source domain; 3) the coefficient shape divergence between the target and source domain; 4) the truncation error $\sum_{d>D+1} \xi_{nd}^{(0)} b_{0d}$; and 5) the sample sizes $N_{\mathcal{A}}$ and N_0 . The following theorems encapsulate these findings on the convergence behavior of the final estimator, in which the function

$$g(x) = \begin{cases} x^{\frac{\alpha_0+2\tilde{\alpha}_0-1}{\alpha_1+2\tilde{\alpha}_0}}, & \text{if } \alpha_1 - \alpha_0 > -1 \\ x \log D, & \text{if } \alpha_1 - \alpha_0 = -1 \\ x, & \text{if } \alpha_1 - \alpha_0 < -1 \end{cases}$$

is used to recast the key factors, and D is chosen to achieve the optimal convergence rate.

Theorem 1. Under Assumption (A1) and (A2), if $s_{\alpha_0-\alpha_1}(D)D^{\alpha_0+2\tilde{\alpha}_0-1} \asymp a_0^{-2}(N_{\mathcal{A}} + N_0)$ and $|\omega_0|D \leq |\omega_1|s_{\alpha_0-\alpha_1}(D)$, then for any $\delta > 0$, with probability greater than $1 - 3\delta$, it holds that

$$\|\hat{\beta}^{(0)} - \beta^{(0)}\|_{\mathcal{C}_0}^2 \lesssim r_1 g\left(\frac{a_0^2}{N_{\mathcal{A}} + N_0}\right) + \tilde{\lambda}^2 \|\beta^{(0)}\|^2 + \frac{r_1}{N_0},$$

where $r_1 = 2\sigma^2 \log(2\delta^{-1})$.

Now we explain the imposed conditions. When $|\omega_0|D \leq |\omega_1|s_{\alpha_0-\alpha_1}(D)$, the upper bound is primarily determined by the source domain, and when $s_{\alpha_0-\alpha_j}(D)D^{\alpha_0+2\tilde{\alpha}_0-1} \asymp a_0^{-2}(N_{\mathcal{A}} + N_0)$, the convergence rate of $\|\hat{\beta}^{(0)} - \beta^{(0)}\|_{\mathcal{C}_0}^2$ achieves the optimal convergence rate by balancing the bias (truncation error) and variance (estimation error).

Since $\|\beta^{(0)}\|$ is fixed, the result in Theorem 1 yields the convergence rate $O(g(a_0^2(N_{\mathcal{A}}+N_0)^{-1}) \vee N_0^{-1} \vee \tilde{\lambda}^2)$. The function $g(\cdot)$ reflects how the difference in the coefficient magnitude and the spectral decay rates between the two domains influence the effectiveness of knowledge transfer. In particular, when the spectral decay rate of $\mathcal{C}_0(\cdot)$ is faster than that of $\mathcal{C}_1(\cdot)$, the benefit of transfer learning becomes more pronounced. For example, if $\alpha_1 - \alpha_0 < -1$ and a_0 is fixed, the convergence rate can be improved to $O((N_{\mathcal{A}} + N_0)^{-1})$. Conversely, if $\mathcal{C}_1(\cdot)$ exhibits a faster spectral decay rate than $\mathcal{C}_0(\cdot)$, the estimation accuracy may deteriorate due to a low signal-to-noise ratio along the leading functional principal components.

The following theorem establishes the convergence rate of the estimation error $\|\hat{\beta}^{(0)} - \beta^{(0)}\|^2$, and similar phenomena are also observed.

Theorem 2. Under Assumption (A1) and (A2), let $D \asymp \{a_0^{-2}(N_{\mathcal{A}} + N_0)\}^{\frac{1}{\alpha_1 + 2\tilde{\alpha}_0}}$, if

$$|\omega_0|D^{\alpha_0+1} \leq |\omega_1|D^{\alpha_1+1} \text{ and } a_0^2 s_{\alpha_0 - \alpha_1}(D)(N_{\mathcal{A}} + N_0)^{-1} + \tilde{\lambda}^2 \ll 1,$$

then for any $\delta > 0$, with probability greater than $1 - 3\delta$, it holds that

$$\|\hat{\beta}^{(0)} - \beta^{(0)}\|^2 \lesssim r_1 \left(\frac{a_0^2}{N_{\mathcal{A}} + N_0} \right)^{\frac{2\tilde{\alpha}_0 - 1}{\alpha_1 + 2\tilde{\alpha}_0}} + \left(\tilde{\lambda}^2 + \frac{r_1}{N_0} \right) \|\beta^{(0)}\|^2,$$

where $r_1 = 2\sigma^2 \log(2\delta^{-1})$.

The result in Theorem 2 yields the convergence rate $O(\{a_0^{-2}(N_{\mathcal{A}} + N_0)\}^{-\frac{2\tilde{\alpha}_0 - 1}{\alpha_1 + 2\tilde{\alpha}_0}} \vee \tilde{\lambda}^2 \vee N_0^{-1})$. The condition $|\omega_0|D^{\alpha_0+1} \leq |\omega_1|D^{\alpha_1+1}$ ensures that the source domain dominates the estimation error. The condition $a_0^2 s_{\alpha_0 - \alpha_1}(D)(N_{\mathcal{A}} + N_0)^{-1} + \tilde{\lambda}^2 \ll 1$ restricts $\tilde{\lambda}$ and $\|\beta^{(1)}\|^{-1}$ from becoming excessively large.

Another insight from these theorems is that, including auxiliary models with weak signal strength (low coefficient magnitude) may increase estimation uncertainty. Specifically, the inclusion of such models reduces $\|\beta^c\|$ resulting in a large value of a_0 . For example, when $|\omega_1| \approx 1$ and $\tilde{\lambda} \approx 0$, $a_0 \approx \|\beta^{(0)}\|/\|\beta^{(1)}\|$. When $\beta^{(1)}(t)$ diminishes, the corresponding source domain provides negligible information, and its inclusion may inflate estimation error rather than reduce it. The last term in the upper bounds, $O(N_0^{-1})$, serves as the baseline error. As $\|\beta^{(j)}\| \rightarrow \infty$ and $\tilde{\lambda} \rightarrow 0$, the first two terms vanish, yet the overall estimation/prediction error does not diminish to zero accordingly due to the error introduced by estimating a_0 .

In the following theorems, we establish the minimax-optimal convergence rate in the transfer learning setting. Notationally, let $r_a = a_1^2/a_0^2$.

Theorem 3. Suppose that the assumptions in Theorem 1 hold, and

$$|\omega_0| + r_a(1 - |\omega_1|) \lesssim r_a^{\frac{2\tilde{\alpha}_0}{\alpha_1 + 2\tilde{\alpha}_0}} (N_0 + N_{\mathcal{A}})^{-\frac{\alpha_1}{\alpha_1 + 2\tilde{\alpha}_0}}, \quad (2-1)$$

then if $\tilde{\lambda}^2 \lesssim N_0^{-\frac{\alpha_0 + 2\tilde{\alpha}_0 - 1}{\alpha_0 + 2\tilde{\alpha}_0}}$, the following result holds,

$$\inf_{\hat{\beta}^{(0)}} \sup_{\beta^{(0)} \in \Theta_{\beta}} \mathbb{P} \left\{ \|\hat{\beta}^{(0)} - \beta^{(0)}\|_{\mathcal{C}_0}^2 \gtrsim \{r_a(N_{\mathcal{A}} + N_0)\}^{-\frac{\alpha_0 + 2\tilde{\alpha}_0 - 1}{\alpha_1 + 2\tilde{\alpha}_0}} + \tilde{\lambda}^2 + N_0^{-1} \right\} > \frac{1}{4}.$$

Theorem 4. Suppose that the assumptions in Theorem 2, along with condition (2-1), hold, then if $\tilde{\lambda}^2 \lesssim N_0^{-\frac{2\tilde{\alpha}_0 - 1}{\alpha_0 + 2\tilde{\alpha}_0}}$, the following result holds,

$$\inf_{\hat{\beta}^{(0)}} \sup_{\beta^{(0)} \in \Theta_{\beta}} \mathbb{P} \left\{ \|\hat{\beta}^{(0)} - \beta^{(0)}\|^2 \gtrsim \{r_a(N_{\mathcal{A}} + N_0)\}^{-\frac{2\tilde{\alpha}_0 - 1}{\alpha_1 + 2\tilde{\alpha}_0}} + \tilde{\lambda}^2 + N_0^{-1} \right\} > \frac{1}{4}.$$

To analyze the impact of source domain, we impose the condition (2-1), under which the source domain predominantly influences the estimation and prediction in the target domain. The condition on $\tilde{\lambda}^2$ restricts the maximum shape misalignment from being excessively large. This condition is natural; otherwise, estimation should rely solely on the target domain, since incorporating the source domain — when it exhibits large bias — would degrade the overall estimation accuracy.

Theorem 4 implies that the convergence rate of estimation error in Theorem 2 is minimax optimal under mild conditions. Notably, when $N_{\mathcal{A}} \gg N_0$, we have $\beta^c(t) \approx \beta^{(1)}(t)$, which implies $r_a \approx a_0^{-2}$. While the convergence rate of the prediction error is not guaranteed to be minimax optimal, it is so when $\alpha_1 > \alpha_0 - 1$. When $\alpha_1 = \alpha_0 - 1$, the quantity $r_a(N_{\mathcal{A}} + N_0)^{-\frac{\alpha_0 + 2\tilde{\alpha}_0 - 1}{\alpha_1 + 2\tilde{\alpha}_0}}$ simplifies to approximately $a_0^2(N_{\mathcal{A}} + N_0)^{-1}$. This differs from the rate of the proposed estimator only by a logarithmic factor (i.e., a “log D ” term). In comparison, the minimax convergence rate of prediction error based solely on the target domain is $N_0^{-\frac{\alpha_0 + 2\tilde{\alpha}_0 - 1}{\alpha_0 + 2\tilde{\alpha}_0}}$. Even in the non-optimal case ($\alpha_1 < \alpha_0 - 1$), the final estimator still outperforms the minimax-optimal estimator based solely on the target domain — even when the sample size in the target domain is increased to $N_0 + N_{\mathcal{A}}$, as long as $\alpha_1 < \alpha_0$ and r_a either converges to zero or remains bounded. This highlights the advantage of borrowing information from “high-quality” source domains rather than collecting new target-domain data, which may be expensive or impractical.

2.4.2 Heterogeneous Design

In this section, we investigate the convergence rate of the final estimate in the general scenario where $\{\mathcal{C}_j(\cdot) : j \in \mathcal{A}\}$ are not necessarily well aligned with $\mathcal{C}_0(\cdot)$ and there are multiple source domains. Let $\Sigma_j = N_j^{-1} \Xi_j^\top \Xi_j$, where $\Xi_j = (\xi_1^{(j)}, \dots, \xi_{N_j}^{(j)})^\top$ being non-random, $\xi_n^{(j)} = (\xi_{n1}^{(j)}, \dots, \xi_{nD}^{(j)})^\top$ and $\xi_{nd}^{(j)} = \langle X_n^{(j)}, \nu_d \rangle$. Here we use the matrix $\Sigma_j^{-1/2} \Sigma_0 \Sigma_j^{-1/2}$ to evaluate the spectral misalignment between Σ_0 and Σ_j and denote $\rho_{j,\max}$ as the maximal eigenvalue of $\Sigma_j^{-1/2} \Sigma_0 \Sigma_j^{-1/2}$, and let $\mathcal{R}_j = \sum_{d \geq D+1} \xi_{nd}^{(j)} b_{jd}$ for $j \in \mathcal{A}$ and $\mathcal{R}_0 = 0$. The following theorem establishes the convergence rate of the final estimate under the heterogeneous design.

Theorem 5. Suppose that Assumptions (A1) and (A2) hold. Then for arbitrary $\delta > 0$ and threshold $\tilde{\lambda} \in [0, 1)$, with probability greater than $1 - (|\mathcal{A}| + 2)\delta$, it holds that $\|\hat{\beta}^{(0)} - \beta^{(0)}\|_{\mathcal{C}_0}^2 \lesssim \tilde{S}_1 + \tilde{S}_2 + \tilde{S}_3 + \tilde{S}_4$, where

$$\tilde{S}_1 = a_0^2 \sum_{j \in \mathcal{A} \cup \{0\}} \omega_j^2 \rho_{j,\max} \left(\frac{r_2}{N_j} + \mathcal{R}_j^2 \right), \quad \tilde{S}_2 = \tilde{\lambda}^2 \|\beta^{(0)}\|^2, \quad \tilde{S}_3 = \frac{r_1}{N_0}, \quad \tilde{S}_4 = D^{-(\alpha_0 + 2\tilde{\alpha}_0 - 1)},$$

where $r_2 = 8\sigma^2(D \log 6 + \log \delta^{-1})$.

In Theorem 5, the term $\rho_{j,\max}$ reflects the divergence in spectral decay rate between the j -th source domain and the target domain, and an additional term \mathcal{R}_j^2 arises in \tilde{S}_1 because,

under the heterogeneous design, the model truncation error is not necessarily orthogonal to the leading covariate scores. The first component, \tilde{S}_1 reflects the estimation error of the coefficient shape component $\beta^c(t)$. The second component, \tilde{S}_2 pertains to the bias caused by shape divergence between the source and target domains. The third component \tilde{S}_3 corresponds to the estimation error of the coefficient amplitude a_0 . The final component \tilde{S}_4 accounts for the truncation error of the target model.

3 Informative Set Identification

3.1 Identification through Regularization

When \mathcal{A} is unknown, we develop a data-driven procedure to identify it. In principle, the shape misalignment between $\beta^{(0)}(t)$ and $\{\beta^{(j)}(t): j \in \mathcal{A}\}$ should be small, and thus we propose to minimize the following objective function over $\boldsymbol{\beta}(t) \triangleq \{\beta^{(j)}(t): j = 0, \dots, p\}$

$$S(\boldsymbol{\beta}(t), \lambda) = \frac{1}{2} \sum_{j=0}^p \sum_{n=1}^{N_j} \{y_n^{(j)} - \langle X_n^{(j)}, \beta^{(j)} \rangle\}^2 + \sum_{j=1}^p J_\lambda(\|\mathcal{M}_j\|),$$

where $J_\lambda(\cdot)$ is a concave penalty function such as the smoothly clipped absolute deviation penalty $J_\lambda(x) = \int_0^{|x|} \lambda \min\{1, \frac{(\gamma\lambda-t)_+}{(\gamma-1)\lambda}\} dt$ (SCAD, see Fan and Li [11]) and minimax concave penalty $J_\lambda(x) = \min\{\lambda|x| - x^2/2\gamma, \gamma\lambda^2/2\}$ (MCP, see Zhang [34]). The concavity property is important for guaranteeing the consistency of informative set identification (see also Jiao and Chan [18], Ma and Huang [23] and Shen and Huang [28]). The penalty term incorporates all the coefficient shape misalignments between the source domains and the target domain and shrinks insignificant coefficient shape misalignments, aiding in the identification of the informative set.

Since $S(\boldsymbol{\beta}(t), \lambda)$ involves elements of infinite dimensions, we minimize the following truncated version over $\{b_{jd}: d = 1, \dots, D, j = 0, \dots, p\}$ to obtain the regularized estimates $\{\hat{b}_{jd}: d = 1, \dots, D, j = 0, \dots, p\}$,

$$S_D(\boldsymbol{\beta}(t), \lambda) = \frac{1}{2} \sum_{j=0}^p \sum_{n=1}^{N_j} \left(y_n^{(j)} - \sum_{d=1}^D b_{jd} \xi_{nd}^{(j)} \right)^2 + \sum_{j=1}^p J_\lambda(\|\mathbf{M}_j\|), \quad (3-1)$$

where $\mathbf{M}_j = \{M_{dd'}^{(j)}, 1 \leq d < d' \leq D\}$. Then $\{\widehat{\mathbf{M}}_j: j \geq 1\}$ from $\{\hat{b}_{jd}^{(\lambda)}: 1 \leq d \leq D, j \geq 0\}$ are constructed from the estimated coefficients as $\widehat{M}_{dd'}^{(j)} = \hat{b}_{jd}^{(\lambda)} \hat{b}_{0d'}^{(\lambda)} - \hat{b}_{jd'}^{(\lambda)} \hat{b}_{0d}^{(\lambda)}$. We then identify the informative set as $\widehat{\mathcal{A}} = \{j: \|\widehat{\mathbf{M}}_j\| \leq \tilde{\lambda} \|\hat{\mathbf{b}}_j^{(\lambda)}\| \|\hat{\mathbf{b}}_0^{(\lambda)}\|\}$, where $\hat{\mathbf{b}}_j^{(\lambda)} = (\hat{b}_{j1}^{(\lambda)}, \dots, \hat{b}_{jD}^{(\lambda)})$. The optimization problem in (3-1) can be solved using a linearized ADMM algorithm (see the supplementary material).

A grid search over $(\lambda, \tilde{\lambda})$ yields a sequence of candidate informative sets for $\widehat{\mathcal{A}}$. Each candidate is evaluated via a bootstrap procedure: the target coefficient $\beta^{(0)}(t)$ is estimated

using transfer learning, residuals $\hat{\epsilon}_n = y_n^{(0)} - \hat{y}_n^{(0)}$ are computed, and bootstrap responses $\tilde{y}_n^{(0)} = \hat{y}_n^{(0)} + \hat{\epsilon}_n^*$ are generated, where $\hat{\epsilon}_n^*$ is obtained by resampling $\hat{\epsilon}_n$ with replacement. The model is then refitted to obtain a bootstrap estimate, and the mean squared prediction error (MSE) is calculated. This process is repeated (e.g., 1000 times) to compute the average MSE for each candidate set. The final informative set $\hat{\mathcal{A}}$ is selected as the one minimizing the average MSE. After identifying the informative set, a post-selection procedure can be applied to remove source domains with significantly slower spectral decay rates and small coefficient magnitudes.

3.2 Identification Consistency

In this section, we investigate the consistency of the identified informative set. We establish the conditions on the tuning parameters, coefficient shape misalignment, and the dimension D required to accurately find \mathcal{A} . We demonstrate that, under these regularity conditions, there exists a local minimizer of the objective function (3-1) such that the associated informative set matches the true one with high probability. Before presenting the main theoretical results, we first introduce the following assumption:

- (A3) $J_\lambda(t)$ is a non-decreasing and concave function for $t \in [0, \infty)$ and $J_\lambda(0) = 0$. There exists a constant $\gamma > 0$ such that $J_\lambda(t)$ is constant for all $t \geq \gamma\lambda \geq 0$. The gradient $J'_\lambda(t)$ exists and is continuous except for a finite number of t and $\lim_{t \rightarrow 0^+} J'_\lambda(t) = \lambda$.

Assumption (A3) holds for many concave penalty functions such as SCAD penalty and MCP. By the results in Section 2.4, the tuning parameter $\tilde{\lambda}$ should converge to zero to ensure consistent final estimates. Notably, as $\tilde{\lambda} \rightarrow 0$, $\beta^{(j)}(t) \rightarrow a_j \beta^c(t)$ for $j \in \mathcal{A}$. We show that under some regularity conditions there is a local minimizer of (3-1) around $\mathbf{B}^0 = (\mathbf{b}_0^0, \dots, \mathbf{b}_p^0)$, where $\mathbf{b}_j^0 = (b_{j1}^0, \dots, b_{jD}^0)$ and

$$b_{jd}^0 = \begin{cases} \langle a_j \beta^c, \nu_d \rangle, & \text{if } j \in \mathcal{A} \cup \{0\}, \\ \langle \beta^{(j)}, \nu_d \rangle, & \text{if } j \notin \mathcal{A} \cup \{0\}, \end{cases}$$

so that the associated identified set coincides with the true informative set with high probability as the sample sizes $\{N_j : j \in \mathcal{A} \cup \{0\}\}$ diverge. Clearly, \mathbf{B}^0 is constructed in accordance with the definition of the informative set \mathcal{A} , and \mathbf{b}_j^0 shares exactly the same coefficient shape as \mathbf{b}_0^0 for $j \in \mathcal{A}$.

Let $\{\mathbf{M}_j^0 : j \geq 1\}$ represent the coefficient shape misalignment associated with \mathbf{B}^0 , and $\tau_N = \sqrt{N^{-1} \log N}$. The notation \mathcal{R}_j is introduced in Section 2.4.2. The following theorem is about the consistency of $\hat{\mathcal{A}}$.

Theorem 6. Under Assumptions (A1), (A2) and (A4), if the following two conditions hold,

- C1). $\|\mathbf{M}_j^0\| - 2(\tau_{N_0} \tau_{N_j} + \tau_{N_0} \|\mathbf{b}_j^0\| + \tau_{N_j} \|\mathbf{b}_0^0\|) > \max\{\gamma\lambda, \tilde{\lambda}(\|\mathbf{b}_j^0\| + \tau_{N_j})(\|\mathbf{b}_0^0\| + \tau_{N_j})\}$, for $j \notin \mathcal{A}$,

$$\text{C2). } \lambda \tilde{\lambda} \|\mathbf{b}_0^0\| \left(\sum_{j \in \mathcal{A}} \|\mathbf{b}_j^0\| \right) \gg \max_{j=0, \dots, p} (\log N_j + \sqrt{N_j \log N_j} \{ \mathcal{R}_j + \tilde{\lambda} \|\beta^{(j)}\| \}),$$

$$\text{C3). } \frac{\sum_{i \in \mathcal{A}} a_i}{\sum_{i \in \mathcal{A} \cup \{0\}} a_i} - 1 < c < 0 \text{ and } \sum_{j \in \mathcal{A}} \left(\frac{\sum_{i \in \mathcal{A} \cup \{0\}, i \neq j} a_i}{\sum_{i \in \mathcal{A} \cup \{0\}} a_i} - 1 \right) < c < 0,$$

then, when $\{N_j: j = 0, \dots, p\}$ are sufficiently large, there exists a local minimizer of (3-1) around \mathbf{B}^0 satisfying that

$$P(\hat{\mathcal{A}} \neq \mathcal{A}) \leq 2D \sum_{j=0}^p N_j^{-1},$$

where $\hat{\mathcal{A}}$ is the identified informative set associated with the minimizer.

Theorem 6 shows that if $i \in \mathcal{A}$, the probability of excluding the i -th source domain from $\hat{\mathcal{A}}$ decreases at a rate of D/N_i . As a result, if $D/N_i \rightarrow 0$ as $N_i \rightarrow \infty$, the probability of correctly including the i -th source domain in $\hat{\mathcal{A}}$ converges to 1.

Conditions C1) and C2) depend not only on the tuning parameters but also on the coefficient magnitudes. C1) highlights the crucial role of the concavity of $J_\lambda(\cdot)$. As the parameter γ increases, the concavity of the penalty function $J_\lambda(\cdot)$ becomes less influential, potentially leading to a violation of C1). Concavity plays a crucial role in distinguishing substantial shape misalignments from minor variations by reducing over-shrinkage, thereby improving the accuracy in identifying the true informative set. C2) implies that, for a shape discrepancy to be detectable, it must be sufficiently pronounced relative to the coefficient magnitude, estimation error, and truncation error. \mathcal{R}_j is removed from C2) under the homogeneous setting. C3) imposes a regularization constraint on the magnitude of the coefficients to avoid extremely large or small value of $\|\beta^{(0)}\|$ relative to the overall scale.

4 Simulation Studies

4.1 General Setting

In this section, we study the finite-sample properties of the developed methodologies through numerical experiments. Here we focus on the estimation error, as the main factors discussed in Section 2.4 influence the prediction error in a similar manner. We omit the intercept, since it is not of major interest. We consider the following three settings.

Setting 1. We simulate data from the functional regression models

$$y_n^{(j)} = \langle X_n^{(j)}, \beta^{(j)} \rangle + \epsilon_n^{(j)},$$

where $\epsilon_n^{(j)} \stackrel{i.i.d.}{\sim} \mathcal{N}(0, s^2)$. The functional covariates and the coefficient functions are generated from the following basis expansion, $\beta_j(t) = \sum_{d=1}^D b_{jd} \nu_d(t)$, $X_n^{(j)}(t) = \sum_{d=1}^D \xi_{nd}^{(j)} \nu_d(t)$, $\xi_{nd}^{(j)} \sim \mathcal{N}(0, d^{-1.2 \times 2})$, where $\{\nu_d(t): d \geq 1\}$ are Fourier basis functions.

The coefficient scores $\{(b_{j1}, \dots, b_{jD}), j = 0, \dots, 9\}$ are generated based on three different templates: $\text{Temp}_1 = B_1/\|B_1\|$, $\text{Temp}_2 = B_2/\|B_2\|$ and $\text{Temp}_3 = B_3/\|B_3\|$, where $B_1 = \{3, 3 - \tau, \dots, 1 + \tau, 1, 1 + \tau, \dots, 3 - \tau, 3\}$, $\tau = 4/(D - 1)$, $B_2 = \{2^{-d}: d = 1, \dots, D\}$, and $B_3 = \{1.2^{-d}: d = 1, \dots, D\}$. The coefficient scores are then generated according to the following scheme:

$$\begin{aligned} \text{For } j = 0, 1, \dots, 5: \{b_{j1}, \dots, b_{jD}\} &= f_j \times \text{Temp}_1 && \text{(V-shape)} \\ \text{For } j = 6, 7: \{b_{j1}, \dots, b_{jD}\} &= f_j \times \text{Temp}_2 && \text{(fast-decay)} \\ \text{For } j = 8, 9: \{b_{j1}, \dots, b_{jD}\} &= f_j \times \text{Temp}_3 && \text{(slow-decay)} \end{aligned}$$

where $\{f_j: j = 0, 1, \dots, 9\} = (3.0, 3.9, 4.8, 3.0, 3.9, 4.8, 3.6, 3.0, 3.9, 4.8)$. The three template scores for $D = 11$ are shown in Figure 1.

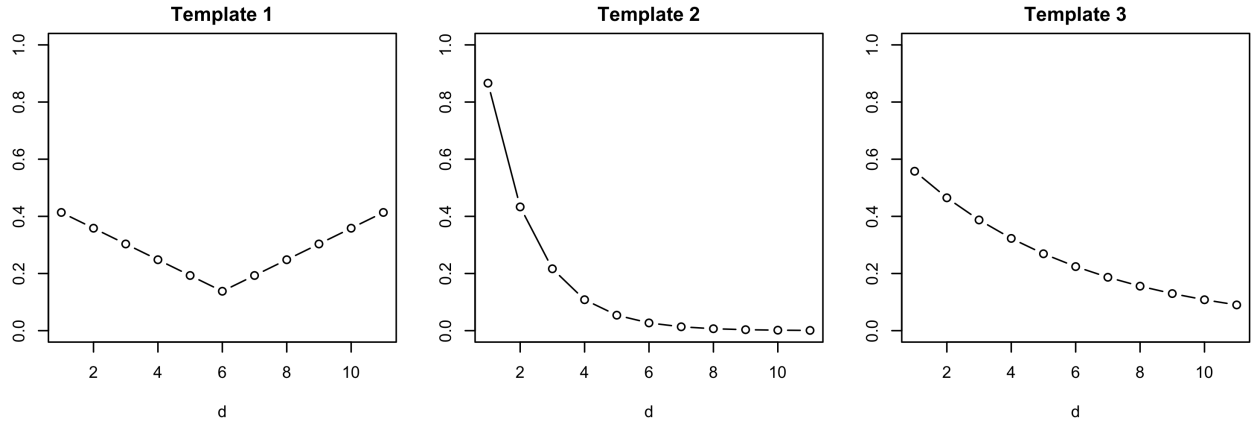


Figure 1: Three templates coefficient scores in Setting 1 ($D = 11$).

The coefficient function of the target model is determined by B_1 . To investigate the impact of non-informative source domains, we designate the 6-th to 9-th source domains as non-informative. The oracle informative set consists of the 1-st to 5-th source domains.

Setting 2. We simulate data from the following functional regression models

$$\begin{aligned} y_n^{(0)} &= \langle X_n^{(0)}, \beta^{(0)} \rangle + \epsilon_n^{(0)}, \quad n = 1, \dots, N, \\ y_n^{(1)} &= \langle X_n^{(1)}, \beta^{(1)} \rangle + \epsilon_n^{(1)}, \quad n = 1, \dots, 5N, \end{aligned}$$

where $\epsilon_n^{(j)} \stackrel{i.i.d.}{\sim} \mathcal{N}(0, s^2)$, $j = 0, 1$. The functional covariates $\{X_n^{(j)}(t): j = 0, 1, n \geq 1\}$ and the coefficient functions $\{\beta^{(j)}(t): j = 0, 1\}$ are generated following the same basis expansion as in Setting 1, and $\xi_{nd}^{(0)} \sim \mathcal{N}(0, d^{-1.3 \times 2})$, $\xi_{nd}^{(1)} \sim \mathcal{N}(0, d^{-2\alpha})$, and $\{b_{j1}, \dots, b_{jD}\} = f_j \times \text{Temp}_4$, where $f_0 = 3.29$, $f_1 = 3.76$, and $\text{Temp}_4 = B_4/\|B_4\|$, where $B_4 = \{1.5^{-d}: d = 1, \dots, D\}$.

Setting 3. We simulate data from the following functional regression models

$$y_n^{(0)} = \langle X_n^{(0)}, \beta^{(0)} \rangle + \epsilon_n^{(0)}, \quad n = 1, \dots, N,$$

$$y_n^{(1)} = \langle X_n^{(1)}, \beta^{(1)} \rangle + \epsilon_n^{(1)}, \quad n = 1, \dots, N,$$

where $\epsilon_n^{(j)} \stackrel{i.i.d.}{\sim} \mathcal{N}(0, s^2)$, $j = 0, 1$. The functional covariates $\{X_n^{(j)}(t): j = 0, 1, n \geq 1\}$ and the coefficient functions $\{\beta^{(j)}(t): j = 0, 1\}$ are generated following the same basis expansion as in Setting 1, and $\xi_{nd}^{(j)} \sim \mathcal{N}(0, d^{-1.2 \times 2})$ for $j = 0, 1$, and $\{b_{j1}, \dots, b_{jd}\} = f_j \times \text{Temp}_3$. We set $f_0 = 1$ and allow f_1 vary.

In Setting 1, we examine the impact of informative set identification on estimation performance. Specifically, we evaluate the transfer learning approach under two distinct scenarios: one where \mathcal{A} is known and another where \mathcal{A} is unknown. In Setting 2, we examine the impact of the decay rate of the covariate covariance operator. A smaller value of α is expected to result in a more significant improvement in estimation accuracy. In Setting 3, we study the influence of coefficient magnitude under varying magnitude of the coefficient in the source domain. In each setting, we repeat the simulation runs 1000 times to compute the average rooted mean squared error (RMSE), defined as $\{\int (\hat{\beta}^{(0)} - \beta^{(0)})^2\}^{1/2}$.

4.2 Estimation Enhancement

In this section, we focus on Setting 1 and consider three approaches and compare their estimation performance: the transfer learning approach based on coefficient shape homogeneity (TS), the transfer learning approach based on coefficient homogeneity (TE), and ordinary least squares estimation (OLS). To examine the impact of informative set identification, we implement the transfer learning approach using both the oracle informative set and the identified informative set.

To identify the informative set, we generate additional 200 validation samples and estimate the prediction error for each candidate informative set. The selected the set which yields the minimal RMSE, and the box-plots of the estimation RMSE are shown in Figure 2. In Table 1, we present the average width of the estimation confidence bands at a significance level of 0.05, defined as $S_\alpha = \int \{u_\alpha(t) - l_\alpha(t)\} dt$, where $u_\alpha(t)$ and $l_\alpha(t)$ represent the upper and lower bounds, respectively, at the 0.05 significance level.

Table 1: Width of 95% confidence bands.

N	D	s	TS (oracle)	TS	TE	OLS
50	5	0.5	0.547	0.585	1.024	1.209
		1.0	1.091	1.195	1.788	2.418
	11	0.5	1.390	1.540	3.236	4.206
		1.0	2.812	3.208	5.268	8.412
100	5	0.5	0.388	0.459	0.672	0.817
		1.0	0.777	0.929	1.441	1.635
	11	0.5	0.922	1.159	2.308	2.863
		1.0	1.851	2.161	4.065	5.726

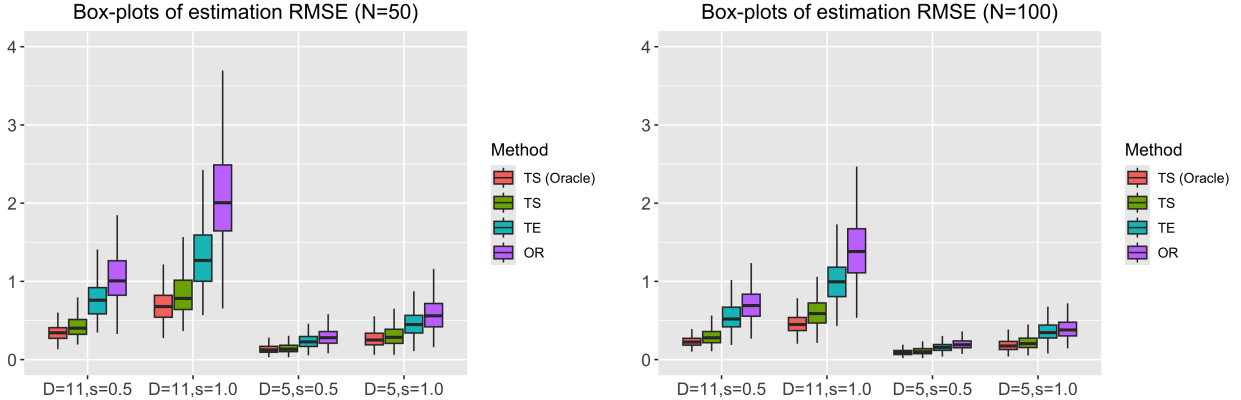


Figure 2: Box-plots of estimation RMSE.

In this setting, the transfer learning estimator that utilizes the full oracle informative set achieves the best overall performance. This is expected, as the covariates across all source domains exhibit identical spectral decay rates and comparable coefficient magnitudes, creating an ideal environment for knowledge transfer. Notably, even without oracle knowledge, the transfer learning approach based on the identified informative set performs nearly as well, demonstrating only a slight degradation in performance due to the uncertainty involved in informative set selection.

Among all competing methods, the transfer learning estimator that leverages coefficient shape homogeneity achieves the best performance, as it flexibly captures shared structural patterns across source domains without requiring identical coefficient magnitudes. In contrast, the approach based on coefficient homogeneity imposes stricter assumptions, which limits its effectiveness when exact similarity does not hold. As expected, the ordinary least squares (OLS) estimator—serving as a baseline that ignores auxiliary information—consistently performs the worst, relying solely on limited target domain data.

These results highlight the advantages of incorporating shape-based transfer mechanisms and confirm the potential gains from accurate informative set identification in multi-source functional regression problems.

4.3 Spectral Decay Rate

In this section, we examine the effect of the spectral decay rate of $\{\mathcal{C}_j(\cdot): j \in \mathcal{A}\}$ and investigate Setting 2. We control the spectral decay rate of $\{\mathcal{C}_j(\cdot): j \in \mathcal{A}\}$ by adapting the value of α . A large value of α leads to a fast spectral decay rate. As discussed in Section 2.4.1, an excessively fast spectral decay rate of covariates in the source domain may degrade estimation performance. The dimension D is chosen as the smallest dimension, for which the cumulative proportion of the eigenvalues of $\mathcal{C}_0(\cdot)$ exceeds 90%.

The estimation RMSEs are displayed in Table 2, which justifies the theoretical findings in Section 2.4.1. It is observed that when the spectral decay rate of the source domain is overly fast, incorporating its data may significantly degrade the estimation performance. When $D = 11$, the deterioration in estimation accuracy due to the source domain is more pronounced, as more dimensions are truncated, leading to a significantly higher truncation bias. This occurs because the negligible variation in the tail covariate scores results in a high estimation error caused by the low signal-to-noise ratio.

Table 2: Estimation RMSE under different spectral decay rates of $\mathcal{C}_1(\cdot)$.

N	D	s	TS					OLS
			$\alpha = 1.1$	$\alpha = 1.3$	$\alpha = 1.5$	$\alpha = 1.7$	$\alpha = 1.9$	
50	5	0.5	0.168	0.190	0.232	0.301	0.401	0.469
		1.0	0.337	0.380	0.464	0.599	0.794	0.938
	11	0.5	0.400	0.531	1.040	2.221	4.425	1.545
		1.0	0.748	1.048	2.049	4.318	7.233	3.081
100	5	0.5	0.124	0.140	0.172	0.222	0.294	0.305
		1.0	0.247	0.281	0.344	0.443	0.586	0.609
	11	0.5	0.267	0.364	0.731	1.599	3.313	0.980
		1.0	0.489	0.731	1.447	3.119	6.000	1.951

4.4 Coefficient Magnitude

In this section, we focus on Setting 3 to examine the performance of the transfer learning framework with varying f_1 . The estimation RMSEs are displayed in Figure 3. The results suggest that a large value of f_1 leads to better estimation, primarily because the source domain helps reduce the scale coefficient. This phenomenon can be explained by the relationship between coefficient magnitude and signal strength. Specifically, a higher coefficient magnitude in the source domain enhances the signal-to-noise ratio, making it easier to extract meaningful information and improving the estimation accuracy in the target domain. Conversely, if the coefficient magnitude in the source domain is too small, the signal is then weak, limiting the benefits of transfer learning and potentially leading to suboptimal estimation in the target domain. As f_1 increases, the average RMSE does not vanish due to the estimation of a_0 .

5 Application

5.1 Background on Wearable Device Data

This paper is motivated by the increasing need to compare groups of subjects in terms of functional health outcomes, particularly in the context of physiological monitoring. Advances

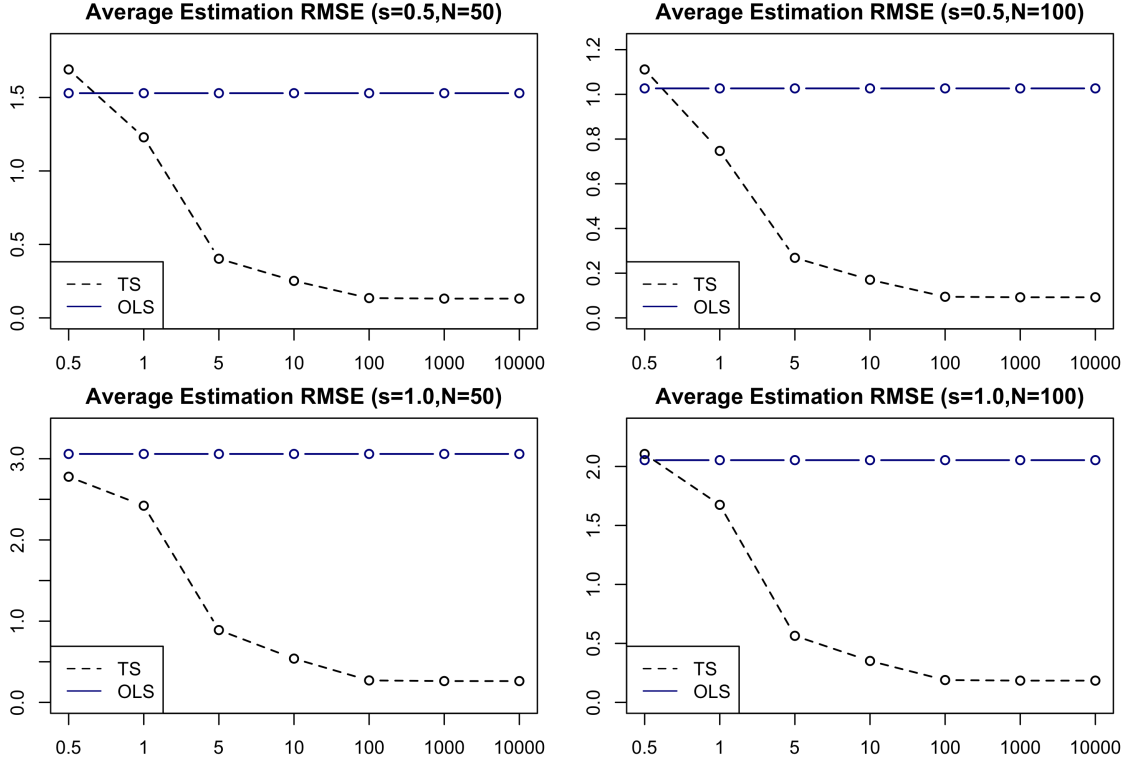


Figure 3: Average Estimation RMSE ($D = 11$). The x-axis represents the values of f_1 .

in wearable sensor technology have made it possible to collect vast amounts of longitudinal data over extended periods (ranging from weeks to months). These sensors are becoming indispensable in a wide array of research areas, including epidemiology, public health, and biomedical studies, such as those focused on congestive heart failure, pulmonary disease, diabetes, obesity, and Alzheimer’s disease. Various functional data analysis methods have been developed to handle such data (see e.g., Zhang et al. [35] and Chang and McKeague [7]).

Here we focus on data collected from wearable devices for monitoring physical activity, which has become a key area of interest in studies of human physiology and pathophysiology (see Wright et al. [32]). Physical activity is often measured by the amount of time spent in various levels of intensity throughout the observation period, as assessed, for example, from data collected as “counts” recorded by ActiGraph devices. Thresholds are commonly applied to sensor readings to define different activity categories (Matthews et al. [24]). However, these thresholds lack justification in the absence of separate validation studies. To address this concern, we move beyond measuring time within discrete activity categories and instead treat activity as a continuum. Specifically, we analyze activity in terms of occupation time, which represents the total duration spent above each activity level as a function of that level across the full range of sensor readings (see also Chang and McKeague [7, 8]).

We use scalar-on-function regression to investigate the association between chronological age and occupation time, using data from the 2005–2006 U.S. National Health and Nutri-

tion Examination Survey (United States National Center for Health Statistics, 2005–2006). This study can help inform public health and medical research by highlighting how physical activity patterns vary across the lifespan, which could be useful for interventions or recommendations related to aging, health, and well-being. Here we split all subjects into 10 separate groups based on their gender and ethnic group. There are five ethnic groups in this dataset, including Mexican American, Other Hispanic, Non-hispanic White, Non-hispanic Black, and other ethnic groups (including multi racial), and two category of genders considered, including male and female.

5.2 Data Pre-processing

We first remove the outliers based on the ℓ^2 -norm of the raw activity curves for the ten groups. The outliers are defined as those beyond the interval $[Q_1 - 1.5 \times \text{IQR}, Q_3 + 1.5 \times \text{IQR}]$. where Q_1, Q_3 are the first, third quantile of the function ℓ^2 -norm, and $\text{IQR} = Q_3 - Q_1$. We transform the raw activity functions into occupation time functions. Occupation time refers to the duration a stochastic process spends within a particular set, such as exceeding a threshold level “ a ”. Let $\{X(t) : t \in [0, T]\}$ be a measurable stochastic process representing the complete observed trajectory of a raw activity curve for a given subject. The occupation time that $X(t)$ spends above the threshold a is defined as: $L(a) = \text{Leb}(\{t \in [0, T] : X(t) > a\})$, where Leb denotes the Lebesgue measure on the real line. The index “ a ” varies over the range of activity levels being studied. As a function of “ a ”, $L(a)$ is bounded between 0 and T , is monotonically decreasing, and is right-continuous by definition. The original occupation time functions for the ten groups are displayed in Figure 4. Then we take the square root transformation for the occupation functions and log-transformation for chronological age to stabilize variance. The log-transformed age and the square-rooted occupation time functions are then used as response and covariate variables respectively.

5.3 Estimation Performance and Comparison

Here, we find that the estimation of models established for Mexican American females (target domain) is significantly improved by the data collected from Mexican American males and Non-Hispanic white males (informative source domains). To evaluate the estimation performance, we applied the Monte Carlo cross-validation procedure (see Picard and Cook [26]). We split the entire dataset into random portions for the training set (75%) and the test set (25%). The target model is estimated based on the training set, which is then used to predict the test set. The steps are repeated for 1000 times. Here we defined the RMSE as follows:

$$\text{RMSE} = \left\{ \frac{1}{N} \sum_{n=1}^N (y_n^{(b)} - \hat{y}_n^{(b)})^2 \right\}^{1/2},$$

where $y_n^{(b)}$ is the responses in the b -th bootstrap repetition, and $\hat{y}_n^{(b)}$ are their predictions. The box-plots of the prediction RMSE are shown in Table 3.

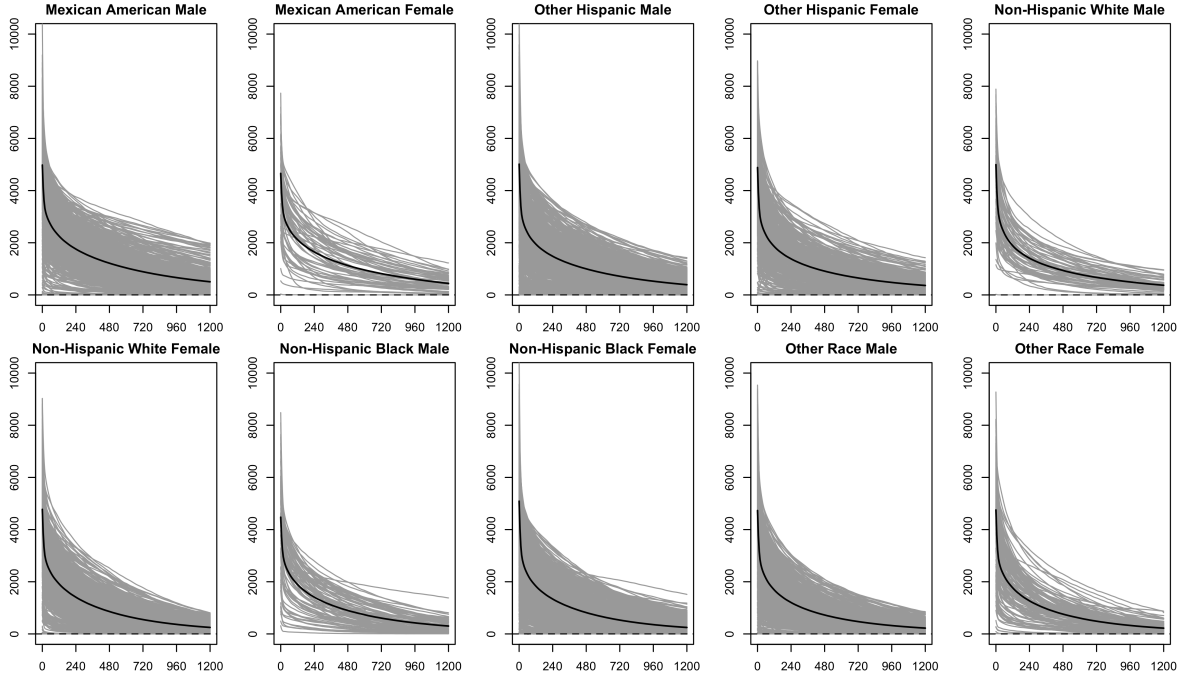


Figure 4: Occupation time functions for the 10 groups of participants. The black curves are the associated average function.

Table 3: Average estimation RMSEs. NA indicating fitting with a model with a zero coefficient function. The values in the parenthesis pertain to the standard deviation of the estimation RMSEs.

Methods	TS	OR	NA
RMSE	0.376(0.055)	0.388(0.059)	0.417(0.056)

We also construct confidence bands to quantify the uncertainty of the estimated functional coefficient in the target domain. To achieve this, we develop a residual-based bootstrap procedure (Algorithm 1, see e.g., González-Manteiga and Martínez-Calvo [13]) that resamples the fitted residuals and refits the model repeatedly to capture the sampling variability of $\hat{\beta}^{(0)}(t)$. This approach allows us to construct pointwise confidence intervals across the entire domain of t . The resulting 95% bootstrap confidence bands provide a visual representation of the estimation uncertainty and are displayed in Figure 5.

Algorithm 1 Bootstrap Confidence Band

- 1: Fit the functional linear model and obtain residuals: $\hat{Y}_i = \int X_i(t)\hat{\beta}^{(0)}(t)dt$, $\hat{\epsilon}_i = Y_i - \hat{Y}_i$.
 - 2: Resample residuals $\hat{\epsilon}_i^*$ with replacement and generate new responses: $Y_i^* = \hat{Y}_i + \hat{\epsilon}_i^*$.
 - 3: Refit the model using bootstrapped responses to get $\hat{\beta}^*(t)$.
 - 4: Repeat steps 2–3 many times (e.g., 1000 times) to obtain an empirical distribution of $\hat{\beta}^*(t)$.
 - 5: Compute pointwise percentiles (e.g., 2.5% and 97.5%) to construct confidence bands.
-

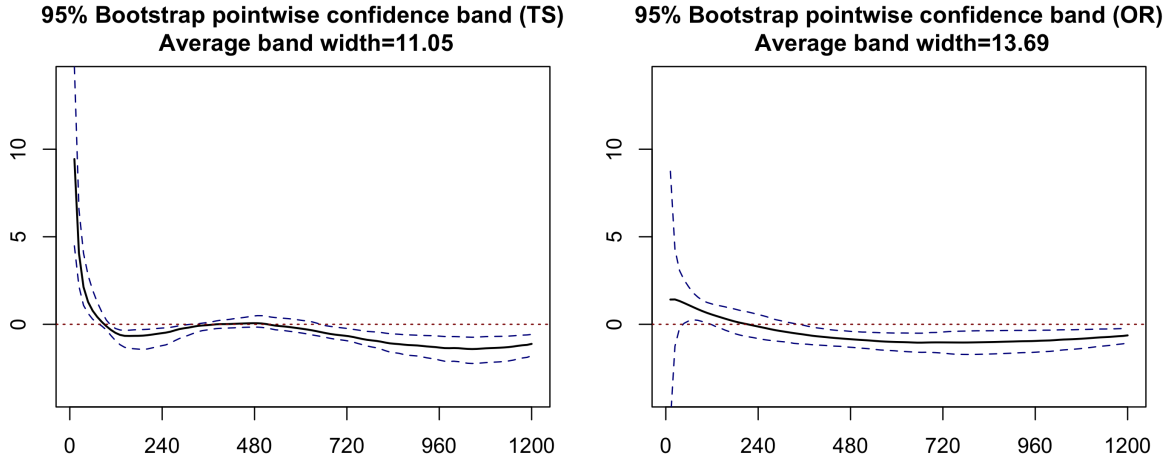


Figure 5: Estimated coefficient function (black line) and the 95% bootstrap pointwise confidence bands (dashed lines).

We found that the transfer learning approach improves the effect size of the target model from 7% to 10% and also narrows the confidence bands of the coefficient function. The pattern of the coefficient function is significantly changed by the source domains. For example, it turns out that the period from 0 to 100 of the occupation time function has a significant effect on the response, whereas the ordinary method leads to the opposite conclusion.

6 Conclusions

We have developed a novel transfer learning framework for functional linear models that leverages coefficient shape similarity to transfer structural information across domains. By shifting the focus from strict coefficient homogeneity to coefficient shape homogeneity, our framework substantially broadens the scope of transferable knowledge, offering a more robust and interpretable foundation for cross-domain inference. This flexibility enables the integration of heterogeneous yet structurally related sources, thereby improving estimation accuracy in the target domain.

The proposed approach proceeds in two main stages. First, we estimate a shared coefficient shape by aggregating information from both the target domain and source domains. In the second stage, we refine this estimated template by multiplying it with a scale parameter to obtain the final estimator of the target coefficient. We rigorously study the convergence properties of the resulting final estimator under both non-random and random designs. Theoretical analysis reveals that the convergence rate is influenced by the sample sizes of different domains, the spectral decay rate of covariate covariance operators, the magnitudes of coefficients, and the shape divergence between the source and target domain coefficients. To address the challenge of unknown informativeness, we develop a source domain selection procedure that identifies informative source domains without relying on prior knowledge. The

practical effectiveness of our method is demonstrated through extensive simulation studies and real data analysis using NHANES physical activity data. The proposed framework, grounded in the concept of coefficient shape homogeneity, provides a flexible foundation for broader applications and can be extended to other functional linear models, including functional autoregressive models and functional factor models. These extensions are nontrivial and will be pursued in future work.

References

- [1] Ardalan, Z. and Subbian, V. [2022], ‘Transfer learning approaches for neuroimaging analysis: a scoping review’, *Frontiers in Artificial Intelligence* **5**, 780405.
- [2] Baker, C. R. and McKeague, I. W. [1981], ‘Compact covariance operators’, *Proceedings of the American Mathematical Society* **83**(3), 590–593.
- [3] Bastani, H. [2021], ‘Predicting with proxies: Transfer learning in high dimension’, *Management Science* **67**(5), 2964–2984.
- [4] Cai, T. T. and Hall, P. [2006], ‘Prediction in functional linear regression’, *The Annals of Statistics* **34**(5), 2159–2179.
- [5] Cai, T. T., Kim, D. and Pu, H. [2024], ‘Transfer learning for functional mean estimation: Phase transition and adaptive algorithms’, *The Annals of Statistics* **52**(2), 654–678.
- [6] Cai, T. T. and Yuan, M. [2012], ‘Minimax and adaptive prediction for functional linear regression’, *Journal of the American Statistical Association* **107**(499), 1201–1216.
- [7] Chang, H.-W. and McKeague, I. W. [2022], ‘Empirical likelihood-based inference for functional means with application to wearable device data’, *Journal of the Royal Statistical Society Series B: Statistical Methodology* **84**(5), 1947–1968.
- [8] Chang, H.-W. and McKeague, I. W. [2024], ‘Concurrent functional linear regression via plug-in empirical likelihood’, *Sankhya A* pp. 1–27.
- [9] Devlin, J., Chang, M.-W., Lee, K. and Toutanova, K. [2019], Bert: Pre-training of deep bidirectional transformers for language understanding, in ‘Proceedings of the 2019 conference of the North American chapter of the association for computational linguistics: human language technologies, volume 1 (long and short papers)’, pp. 4171–4186.
- [10] Du, P. and Wang, X. [2014], ‘Penalized likelihood functional regression’, *Statistica Sinica* **24**, 1017–1041.
- [11] Fan, J. and Li, R. [2001], ‘Variable selection via nonconcave penalized likelihood and its oracle properties’, *Journal of the American statistical Association* **96**(456), 1348–1360.
- [12] Ganin, Y. and Lempitsky, V. [2015], Unsupervised domain adaptation by backpropagation, in ‘International conference on machine learning’, PMLR, pp. 1180–1189.

- [13] González-Manteiga, W. and Martínez-Calvo, A. [2011], ‘Bootstrap in functional linear regression’, *Journal of Statistical Planning and Inference* **141**(1), 453–461.
- [14] Hall, P. and Horowitz, J. L. [2007], ‘Methodology and convergence rates for functional linear regression’, *The Annals of Statistics* **35**(1), 70–91.
- [15] Heinzinger, M., Elnaggar, A., Wang, Y., Dallago, C., Nechaev, D., Matthes, F. and Rost, B. [2019], ‘Modeling aspects of the language of life through transfer-learning protein sequences’, *BMC bioinformatics* **20**, 1–17.
- [16] Hu, X. and Lin, Z. [2025], Transfer learning meets functional linear regression: No negative transfer under posterior drift, in ‘Proceedings of the AAAI Conference on Artificial Intelligence’, Vol. 39, pp. 17351–17358.
- [17] Jiao, S., Aue, A. and Ombao, H. [2023], ‘Functional time series prediction under partial observation of the future curve’, *Journal of the American Statistical Association* **118**(541), 315–326.
- [18] Jiao, S. and Chan, N.-H. [2024], ‘Coefficient shape alignment in multivariate functional regression’, *Journal of American Statistical Association (online)*, <https://doi.org/10.1080/01621459.2024.2422115>.
- [19] Li, S., Cai, T. T. and Li, H. [2022], ‘Transfer learning for high-dimensional linear regression: Prediction, estimation and minimax optimality’, *Journal of the Royal Statistical Society Series B: Statistical Methodology* **84**(1), 149–173.
- [20] Lin, H. and Reimherr, M. [2024], ‘On hypothesis transfer learning of functional linear models’, *Stat* **1050**, 22.
- [21] Liu, H., Men, J., Wang, S., You, J. and Cao, J. [2025], ‘Similarity-informed transfer learning for multivariate functional censored quantile regression’, *arXiv preprint arXiv:2503.18437*.
- [22] Long, M., Cao, Y., Wang, J. and Jordan, M. [2015], Learning transferable features with deep adaptation networks, in ‘International conference on machine learning’, PMLR, pp. 97–105.
- [23] Ma, S. and Huang, J. [2017], ‘A concave pairwise fusion approach to subgroup analysis’, *Journal of the American Statistical Association* **112**(517), 410–423.
- [24] Matthews, C. E., Chen, K. Y., Freedson, P. S., Buchowski, M. S., Beech, B. M., Pate, R. R. and Troiano, R. P. [2008], ‘Amount of time spent in sedentary behaviors in the united states, 2003–2004’, *American journal of epidemiology* **167**(7), 875–881.
- [25] Mei, S., Fei, W. and Zhou, S. [2011], ‘Gene ontology based transfer learning for protein subcellular localization’, *BMC bioinformatics* **12**, 1–12.
- [26] Picard, R. R. and Cook, R. D. [1984], ‘Cross-validation of regression models’, *Journal of the American Statistical Association* **79**(387), 575–583.

- [27] She, Y., Shen, J. and Zhang, C. [2022], ‘Supervised multivariate learning with simultaneous feature auto-grouping and dimension reduction’, *Journal of the Royal Statistical Society Series B: Statistical Methodology* **84**(3), 912–932.
- [28] Shen, X. and Huang, H.-C. [2010], ‘Grouping pursuit through a regularization solution surface’, *Journal of the American Statistical Association* **105**(490), 727–739.
- [29] Tian, Y. and Feng, Y. [2023], ‘Transfer learning under high-dimensional generalized linear models’, *Journal of the American Statistical Association* **118**(544), 2684–2697.
- [30] Tibshirani, R., Saunders, M., Rosset, S., Zhu, J. and Knight, K. [2005], ‘Sparsity and smoothness via the fused lasso’, *Journal of the Royal Statistical Society Series B: Statistical Methodology* **67**(1), 91–108.
- [31] Wang, J.-L., Chiou, J.-M. and Müller, H.-G. [2016], ‘Functional data analysis’, *Annual Review of Statistics and its application* **3**(1), 257–295.
- [32] Wright, S. P., Brown, T. S. H., Collier, S. R. and Sandberg, K. [2017], ‘How consumer physical activity monitors could transform human physiology research’, *American Journal of Physiology-Regulatory, Integrative and Comparative Physiology* .
- [33] Yuan, M. and Cai, T. T. [2010], ‘A reproducing kernel hilbert space approach to functional linear regression’, *The Annals of Statistics* **38**(6).
- [34] Zhang, C.-H. [2010], ‘Nearly unbiased variable selection under minimax concave penalty’, *The Annals of Statistics* **38**(2), 894–942.
- [35] Zhang, Y., Li, H., Keadle, S. K., Matthews, C. E. and Carroll, R. J. [2019], ‘A review of statistical analyses on physical activity data collected from accelerometers’, *Statistics in biosciences* **11**, 465–476.